Infrared lasers using silicon crystals

M. Ohtsu[1] and T. Kawazoe[2]

[1]Research Origin for Dressed Photon,

3-13-19 Moriya-cho, Kanagawa-ku, Yokohama, Kanagawa 221-0022 Japan

[2]Tokyo Denki University,

5 Senju-Asahi-cho, Adachi-ku, Tokyo 120-8551, Japan

Abstract

This article reviews infrared Si lasers fabricated by using dressed photons and capable of CW operation at room temperature. First, the performance of a basic laser device with a ridge waveguide is reviewed. It shows a single longitudinal-mode oscillation at a wavelength of 1.271 μm, manifested by the phenomenon known as photon breeding. Second, by improving the waveguide structure, a threshold current density as low as 40 A/cm^2 is demonstrated. Third, to realize a high-power Si laser device, a Si crystal with a large cross section, and without a waveguide structure, is employed. By improving the structure of the heat sink, by coating end-facets of the cavity with high-reflection films, and by increasing the cavity length to 30 mm, an optical output power as high as 100 W is obtained under triangular-wave (1 Hz repetition frequency) current injection equivalent to injecting a constant current. The peak wavelength in the multi-mode lasing spectrum is 1.95 μm, which depends on the energies of nine phonons. It is expected that this wavelength can be tuned to 1.3 μm by controlling the wavelength dependence of the reflectivity of the high-reflection films coated on the end-facets. The last part of this article compares the operating principle and performance of the present Si-lasers with those of conventional lasers.

1 Introduction

The authors have succeeded in fabricating light-emitting diodes (LEDs) made of crystalline silicon (Si) using dressed photons (DPs) and demonstrated their operation [1]. The DP is an off-shell quantum field that is created as a result of the interactions of photons, excitons, and phonons in a nanometric space [2]. This article reviews the performance of infrared Si lasers fabricated by applying the principles used in fabricating the LEDs described above [3].

Crystalline Si has been the subject of extensive research for use in fabricating lasers since it shows excellent compatibility with electronic devices [4]. For example, there have been several reports of basic devices that have been demonstrated, including Raman lasers [5] and lasers utilizing quantum size effects in Si [6]. However, parameters such as the operating temperature, efficiency, wavelength, optical power and so forth are still not adequate for

practical adoption of these devices.

Optical gain occurs if the device operation satisfies the Bernard–Duraffourg inversion condition [7]. Furthermore, if the device has an optical cavity structure for confining the emission energy, and if the optical gain is larger than the cavity loss, there is a possibility of laser oscillation occurring as a result of stimulated emission. Section 2 of this article reviews infrared single-mode laser devices that are operated under constant current injection at room temperature. Section 3 reviews infrared high-power laser devices whose output powers reach 100 W. Detailed descriptions on the topics in Section 2 and in the first part of Section 3 have been given in ref. [3]. The second part of Section 3 reviews the results of recent experimental studies carried out after the publication of ref. [3]. Section 4 compares the operating principles and performance of Si-lasers with other conventional lasers. Section 5 summarizes this article.

2 Single-mode lasers

This section reviews the fabrication and operation of single-mode Si-laser devices [8,9]. Section 2.1 is devoted to the basic devices. Section 2.2 reviews an improved device structure for decreasing the threshold current density.

2.1 Basic devices

An As-doped n-type Si crystal was used as a device substrate. The electrical resistivity was 10 Ω cm, and the thickness was 625 μm. A part of this crystal was further doped with B atoms by ion implantation to form a p-type layer. The concentration of B atoms was 1×10^{19} cm^{-3} [9]. After forming a p–n homojunction, an ITO film was deposited on the p-layer side of the Si substrate, and an Al film was deposited on the n-substrate side for use as electrodes in the process of annealing described below. Subsequently, the Si crystal was diced to form a device. For DP-assisted annealing [10]*, the substrate was irradiated with infrared laser light having a photon energy $h\nu_{anneal}$ of 0.94 eV (1.32 μm wavelength) and a power density of 200 mW/cm^2, during which annealing was performed by injecting a forward-bias current of 1.2 A to generate Joule-heat, causing the B atoms to diffuse. With this method, the spatial distribution of the B atoms changes in a self-organized manner, resulting in a distribution suitable for efficiently inducing spontaneous and stimulated emission of photons. Next, the ITO electrode and the Al electrode were removed by etching. Then, a ridge waveguide was fabricated by conventional photolithography. After that, an Al film was deposited by DC

sputtering. The substrate was then polished to a thickness of 100 μm, and an Al film was deposited also on the reverse side of the Si substrate. These Al films were used as electrodes for injecting a current to drive the fabricated laser device. The sample was cleaved to various lengths, and the cleaved end-facets served as cavity mirrors.

(*) This method of annealing has been called DPP (dressed-photon–phonon)-assisted annealing in ref. [10]. However, to make the discussion more general, the present article simply calls it DP-assisted annealing.

Figure 1(a) illustrates the device structure. Secondary ion mass spectrometry measurements confirmed that the active layer formed in the p–n homojunction was located at a depth of 1.5–2.5 μm from the surface of the Si substrate. This corresponds to the bottom of the ridge waveguide. Figure 1(b) shows an SEM image of a fabricated device, from which the width and thickness of the ridge waveguide constituting the cavity were confirmed to be 10 μm and 2 μm, respectively. Several devices were fabricated, whose cavity lengths L were 250–1000 μm.

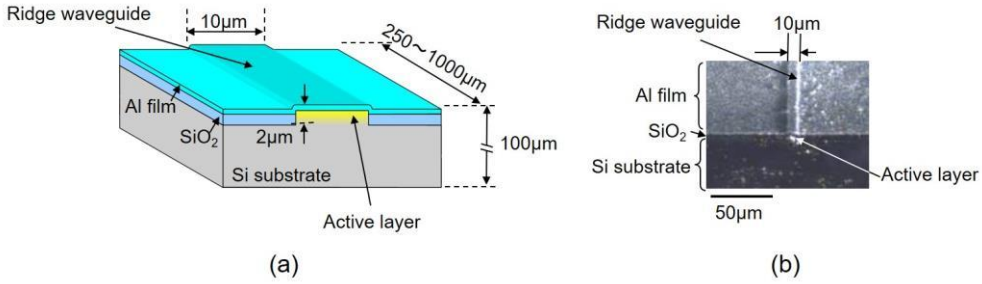

Fig. 1 The profile of a Si laser device.

(a) Schematic illustration of the structure. (b) An SEM image of a fabricated Si laser device.

Figure 2 shows a numerically calculated cross-sectional light intensity profile for the device in Fig. 1. This figure shows that a portion of the light leaked from the active layer, and the optical confinement factor Γ was estimated to be as low as $4.7 \leftrightarrow 10^{-4}$. Due to such weak optical confinement, the optical guiding loss in the ridge waveguide was expected to be as large as 90% or even larger. However, because the DP-assisted annealing formed an active layer that efficiently created DPs, the effective refractive index of the active layer could become higher than the refractive index of the surrounding area. As a result, it was experimentally confirmed that the sum of the optical guiding loss and the optical scattering loss at the end-facets was decreased to 70% for the TE-polarization component.

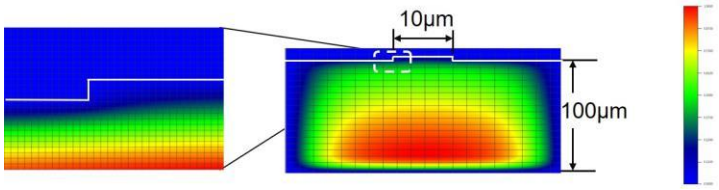

Fig. 2 Calculated cross-sectional light intensity profile for the device in Fig. 1.

All of the experiments described below were conducted at room temperature (15–25 °C). From the measurement of the relation between the injected current density J and the optical gain at a wavelength of 1.32 μm, the transparent current density J_{tr} was evaluated to be 26.3 A/cm^2. This value was about 1/10th that of a conventional laser device made using a direct-transition-type semiconductor [11], demonstrating that the present ridge waveguide with the p–n homojunction structure had adequate performance to be used for the laser device.

Figures 3(a) and (b) respectively show the acquired near-field and far-field images of the optical radiation pattern for the laser with $L = 750$ μm. There is a ridge waveguide with a width of 10 μm at the center of the white broken circle in Fig. 3(a). At an injection current of 50 mA and above, the optical radiation pattern was concentrated inside the ridge waveguide, and the optical power increased (Fig. 3(b)). This concentration indicates that the directivity of the optical radiation pattern was high due to the laser oscillation. At an injection current below 50 mA, on the other hand, the directivity was low because the radiated light is composed of incoherent spontaneous emission and amplified spontaneous emission (ASE).

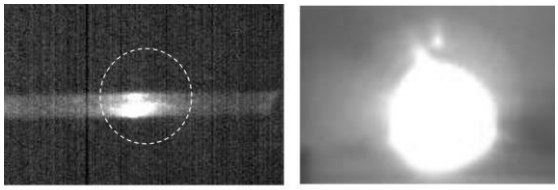

Fig. 3 The optical patterns emitted from the Si laser.
(a) Near-field image. (b) Far-field image.

From the near-field image in Fig. 3(a), it was found that the TM-polarization component spread over the entire device, whereas the TE-polarization component was concentrated in the ridge waveguide. The intensity ratio of the TE- and the TM-polarizations was 8:1. On the other hand, in a conventional semiconductor laser, this ratio is 100:1 or greater [12]. The reason for the difference between these ratios was the absence of an optical confinement structure in the thickness direction of the ridge waveguide in the present device. In the case of

conventional semiconductor lasers, this structure has been formed by using a double-heterojunction structure. Another possible reason was that the spectral wavelength bands of the spontaneous emission and ASE were extremely wide in the present device.

Light emission spectral profiles were measured for the Si laser with L=500 μm. The results are shown in Fig. 4, where the threshold current density J_{th} was 1.1 kA/cm^2. Above the threshold for lasing (at an injection current of 57 mA), a sharp laser oscillation spectrum was observed, as shown in Fig. 4(a). Its wavelength was 1.271 μm, which was evidence of photon breeding [10]. The full width at half maximum (FWHM) was 0.9 nm or less, which was limited by the resolution of the measurement equipment. The sharp spectral peak in Fig. 4(a) represents the CW laser oscillation with a single longitudinal mode that was realized even though the waveguide was as long as 500 μm. Its origin was that the low infrared absorption by the Si provided a low threshold for the principal longitudinal mode at the optical gain spectral peak and, as a result, the gains for other modes were depleted by this principal mode due to nonlinear mode competition [13,14]. Below the threshold (at an injection current of 55 mA (Fig. 4(b)), there existed only a wide, low-power spectrum that originated from the spontaneous emission.

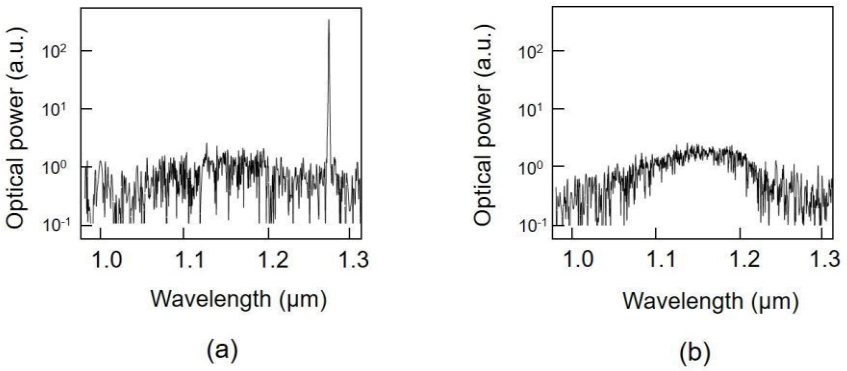

Fig. 4 Light emission spectral profiles of the Si laser with a cavity length of 550 μm.

(a) Above the threshold. (b) Below the threshold.

2.2 Decreasing the threshold current density

This section reviews the design and fabrication of an improved device with a higher optical confinement factor for reducing J_{th} [9]. In designing the device structure, the value of J_{tr} was estimated by using an infrared Si photodetector with optical amplification [15]: By measuring its photocurrent when irradiating it with light having a wavelength of 1.32 μm, J_{tr} was successfully estimated to be 5.0 A/cm^2. Through this estimation, the differential gain

coefficient g was also estimated to be 38.4 cm/A*.

(*) The values of J_{tr} and g have also been estimated by using a different method [16], which has been employed for a conventional infrared laser using a direct transition-type semiconductor [17]. Specifically, the output optical power P_{out} of the light emitted from the output facet of the waveguide was measured by irradiating the input facet of the waveguide with laser light (input optical power P_{in}). The values above were evaluated by the measured values of the ratio P_{out} / P_{in}.

By using these estimated values and the formula in ref. [17], J_{th} was estimated to be 2.6 kA/cm^2, where α_{int}=1.6↔10^{-5} cm^{-1} (internal optical loss coefficient), Γ=4.7↔10^{-4}, L=250 μm, and $R_1 = R_2$=0.31 (reflectivities of the two end-facets of the waveguide) were also used. The value of J_{th} estimated above was close to the measured value given in Section 2.1, confirming the high accuracy of the present estimation.

Since Γ for the device in Fig. 1 was very low (4.7↔10^{-4}), further decreases in J_{th} were expected by increasing Γ. Based on this expectation, the dependence of J_{th} on Γ was numerically calculated, which suggested that J_{th} decreased to less than 1/100th that of the device in Fig. 1, i.e., to 8.8 A/cm^2, by increasing Γ to 0.16.

By following this suggestion and using the numerical values above, an improved device with a larger Γ was designed. Its cross-sectional profile is schematically illustrated in Fig. 5. The device layer was 15 μm thick, which was realized by using a silicon-on-insulator (SOI) substrate. The thickness and width of the ridge waveguide were 2 μm and 8 μm, respectively.

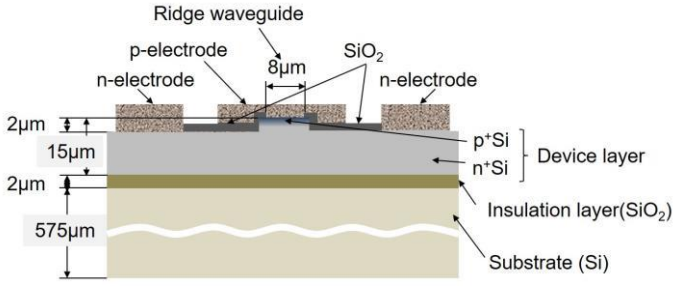

Fig. 5 A cross-sectional profile of the improved device.

Figure 6 shows the numerically calculated cross-sectional light intensity profiles for the device in Fig. 5. A comparison of Figs. 2 and 6 confirms a higher optical confinement factor

Γ in the device in Fig. 5. However, it should be noted that this figure shows that a portion of the lasing light still leaked and spread over a wide area of the device because of its p-n homojunction structure.

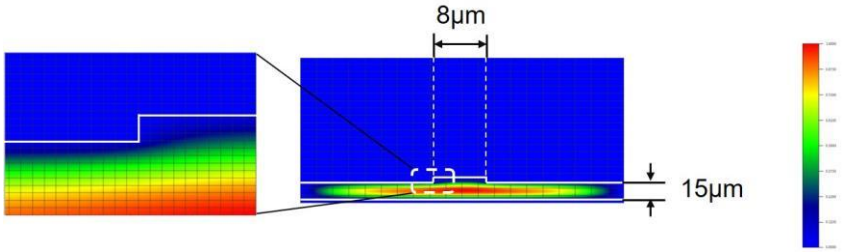

Fig. 6 Calculated cross-sectional light intensity profile for the device in Fig. 5.

The SOI substrate consisted of a device layer, an insulating layer made of SiO_2, and a Si support substrate. The device layer was P-doped n-type Si with a resistivity of 2.0 $\leftrightarrow 10^{-2}$ – $3.4 \leftrightarrow 10^{-2}\ \Omega\ cm$. The thicknesses of the insulation layer and the Si support substrate were 2 μm and 575 μm, respectively.

Some of the fabrication steps were modified from the process in Section 2.1: (1) B ions were doped into the device layer by ion implantation to form a p-type layer. Numerical calculations estimated that a p-n homojunction was located at a depth of 1.5–2.5 μm from the surface of the SOI substrate. (2) A Cr/Pt film was deposited on the surface of the SOI substrate. (3) An electron-beam (EB) resist was coated on the Cr/Pt film layer, and a stripe (8 μm wide) was formed by EB lithography. (4) A Cr/Pt stripe was formed by ICP-RIE etching. (5) The device layer was etched with CF_4 gas to form a ridge waveguide. (6) An SiO_2 film was deposited on the surface of the waveguide to serve as an insulating film. (7) The insulating film on the waveguide and on a part of the device layer surface was removed. (8) The SiO_2 film was etched to expose the top side of the waveguide and part of the device layer surface. (9) A Cr/Pt/Au film was deposited for use as an electrode. Figure 7 shows an SEM image of an end-facet of the waveguides. (10) The SOI substrate was diced to separate each waveguide to form solitary laser devices.

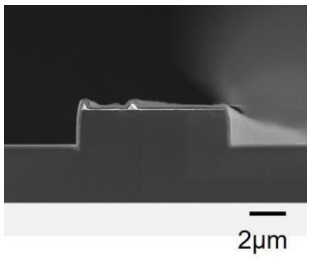

Fig. 7 An SEM image of the end-facet of the waveguide of the fabricated device.

DP-assisted annealing was adopted by injecting a current pulse (1 kHz repetition

frequency, 100 μs pulse width, 77.5 A/cm^2 peak current density, 3.2 V peak voltage). The substrate was irradiated with infrared laser light (1.31 μm wavelength, 1 mW power) during this current injection. The annealing time was 1.5 hours.

Figure 8 shows the light emission spectral profiles that were acquired at room temperature (25 °C). The vertical axis of this graph is a logarithmic scale. Figure 8(a) shows the profile above the threshold for lasing (J =42 A/cm^2). Here, J_{th} was 40 A/cm^2, as will be presented below. The sharp spectral peak at a wavelength of 1.40 μm represents the CW laser oscillation with a single longitudinal mode. Figure 8(b) shows the spectral profile below the threshold (J =38 A/cm^2), in which no ASE spectra are seen because of the gain depletion due to the mode competition described in Section 2.1.

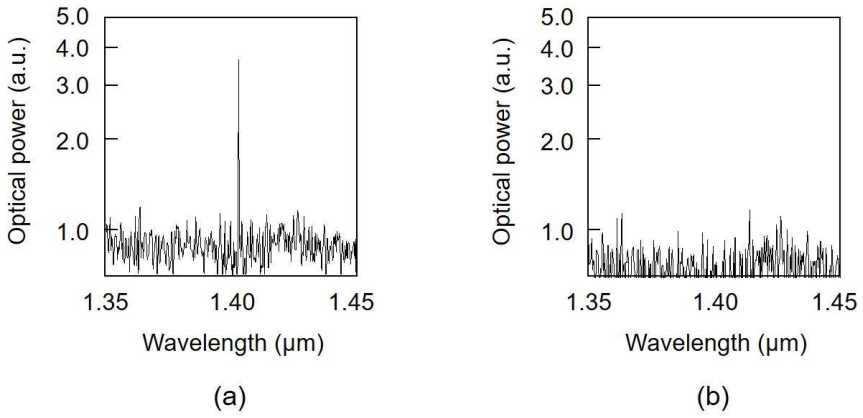

Fig. 8 Light emission spectral profiles.

(a) Above the threshold. (b) Below the threshold.

For accurate estimation of J_{th}, an extremely small current drop in the relation between the applied voltage and J, due to electrical energy being converted to photon energy at the threshold [18], was measured. Figure 9 shows the measured result in which an upward arrow indicates the above-mentioned current drop at 3.0 V. From the value of J at this drop, J_{th} was found to be 40 A/cm^2 [9], which is 1/28th that of the device in Fig. 1.

A possible reason why this value of J_{th} was still higher than the designed value (8.8

A/cm^2) is that the actual value of α_{int} was still higher than the value used for the device design. It should be possible to decrease this value further by improving the fabrication process.

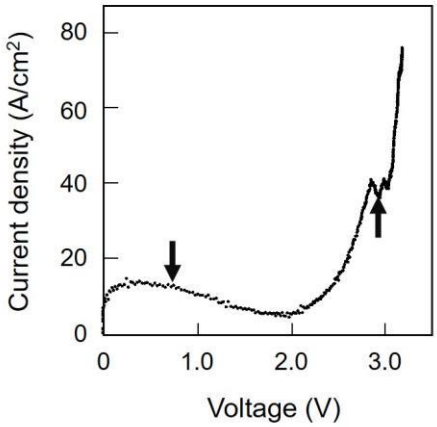

Fig. 9 Relation between the applied voltage and current density.

The upward arrow represents the position of the lasing threshold. The downward arrow represents the negative resistance, which originated from the floating capacitance associated with the electrical circuit used for driving this device.

3 High-power lasers

Section 2 reviewed devices with a narrow ridge waveguide. They realized single-longitudinal mode lasing with a very low J_{th} by constant current injection at room temperature. Due to such prominent features, it was expected that these devices could be used as light sources for information transmission systems, information processing systems, and sensing systems. On the other hand, to apply them to machining and processing systems, high optical output power is required. This section reviews recent progress in fabricating and operating high-power Si laser devices designed to meet this requirement.

Section 2.2 demonstrated that low J_{th} was achieved, which suggested that the present fabrication method had the capability to realize a device with a high optical output power driven by a fairly low J. Based on this suggestion, novel high-power laser devices were designed and fabricated by referring to the values of physical quantities evaluated in

Section 2.2. Here, to ensure a large total optical gain, a Si crystal with a large cross-section and long length, and without a waveguide structure, was employed. Employing such a large Si crystal can be more advantageous than increasing the optical confinement factor of a small waveguide because, and due to the p-n homojunction-structure in the Si crystal, an extremely high optical confinement cannot be expected even by further modification of the waveguide configuration.

Figure 10 shows the cross-sectional structure of the Si crystal used as the laser medium (1 mm width, 150 μm thickness) that was designed for realizing high-power light emission [19]. The length L of the crystal was 15 mm, as seen in the photograph in Fig. 11 (a). The two end-facets of the crystal were cleaved for use as laser cavity mirrors. An As-doped n-type epitaxial Si film (10 μm thickness, 10 Ωcm resistivity) was grown on a Sb-doped n-type Si crystal substrate (15 mΩcm resistivity). A part of this film was further doped with B atoms by ion implantation to form a p-type layer. The concentration of B atoms was 1×10^{19} cm^{-3}. The thickness of the B-doped p-type layer was 1.2 μm. After depositing Cr/Pt/Au films for use as electrodes, the device was installed in a heat sink made of copper plates, as shown in Fig. 11(b). For DP-assisted annealing, one end-facet was irradiated with infrared laser light having $h\nu_{anneal}$ of 0.95 eV (1.31 μm wavelength) and a power of 200 mW, during which annealing was performed by injecting a forward-bias current of 5 A to generate Joule-heat, causing the B atoms to diffuse.

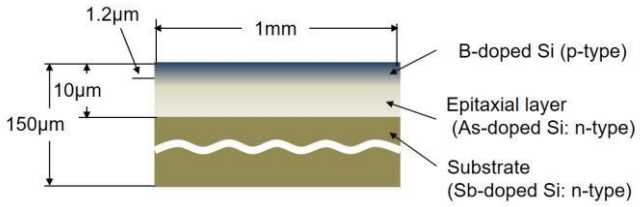

Fig. 10 Cross-sectional profile of the Si crystal used as a laser medium and the laser cavity.

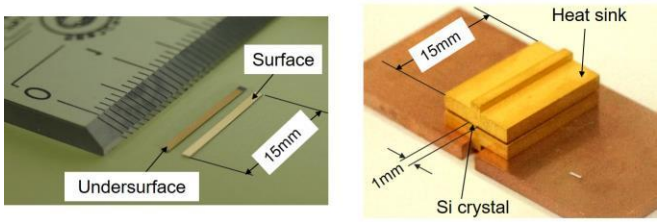

Fig. 11 Photograph of the laser device.

(a) The Si crystal. (b) A heat sink, in which the Si crystal is installed.

By substituting physical quantities evaluated in Section 2.2 into a conventional rate

equation for a laser light intensity, the relation between J and the optical output power P_{out} emitted from one end-facet of the device was derived, as shown in Fig. 12 [19]. This figure shows that J_{th} is about 100 A/cm^2. Since the electrodes may be damaged when J increases to 1 kA/cm^2, which corresponds to the output power of 200 W in Fig. 12, the present study aimed at safely realizing the highest output power of 100 W to avoid the type of damage mentioned above.

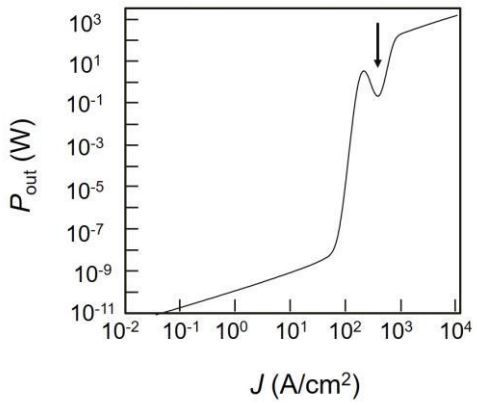

Fig. 12 Calculated relation between J and P_{out} of the fabricated device (L=15 mm).

The downward arrow indicates the dip originating from the saturated absorption feature of the device.

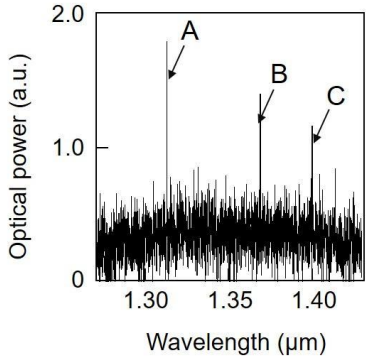

Fig. 13 Light emission spectral profiles.

The wavelength of the spectral peak A is identical to that of the light irradiated during the DP-assisted annealing. The spectral peaks B and C are phonon sidebands, which were generated by creating LO-mode and TO-mode phonons, respectively.

Figure 13 shows the light emission spectral profile above the lasing threshold for lasing under constant current injection at room temperature [20]. In contrast to those in Figs. 4(a) and 8(a), it has three spectral peaks A, B, and C. This multi-wavelength operation was attributed to the multiple transverse and longitudinal modes that were allowed to exist in the present primitive large laser cavity. The spectral peak A is located at a wavelength of 1.31

μm. This is identical to the wavelength of the light irradiated during the DP-assisted annealing, which is direct evidence for photon breeding. The spectral peak B is a phonon sideband, which was generated by creating an LO-mode phonon with an energy of 40 meV at the X-point in the electronic energy band diagram. The spectral peak C is also a phonon sideband, which was generated by creating a TO-mode phonon with an energy of 60 meV.

The closed squares in Fig. 14 represent the measured relation between J and P_{out}. The value of P_{out} took a maximum value of 110 mW at J=33 A/cm^2 (5 A injection current). This value is more than 10-times higher than that of a conventional double heterojunction-structured InGaAsP/InP laser (10 mW at 1.3 μm wavelength: SLT1130 series manufactured by Sumitomo Electric). By taking the optical output power radiated from the other end-facet into account, the maximum total optical output power was 220 mW.

Figure 14 also shows that J_{th} was 12 A/cm^2, which was lower than that described in Section 2.2 (40 A/cm^2). The origin of such a low J_{th} in the present device is attributed to the large total optical gain due to a large laser medium.

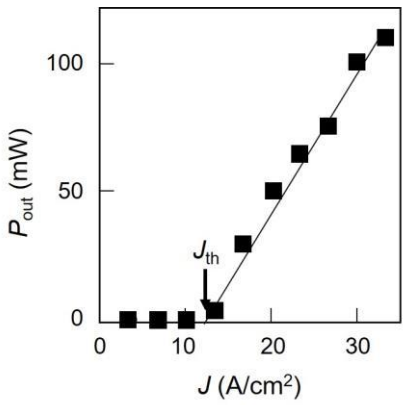

Fig. 14 Measured relation between J and P_{out} emitted from one end-facet of the Si crystal.

The slope of the line fitted to the closed squares indicates that the external differential quantum efficiency was 9.0% in the case where the total optical output power was radiated from the two end-facets. This is higher than the efficiency of a conventional double heterojunction-structured InGaAsP/InP laser (7% at 1.3 μm wavelength: SLT1130 series manufactured by Sumitomo Electric).

Figure 15(a) shows a dazzling infrared radiation pattern from the end-facets, acquired by an infrared camera, which demonstrates the high output optical power. Figure 15(b) is an image of the light scattered from the surface of a screen installed at a position 20 cm away from the laser. The image is spatially modulated, i.e., speckles are clearly seen, which demonstrates a high spatial coherence of the output infrared light beam.

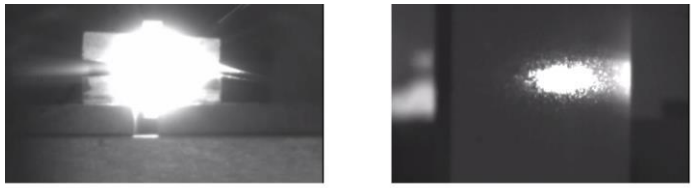

Fig. 15 Images of the output infrared light.

(a) Radiation pattern of the infrared light emitted from the end-facet. (b) The speckles in the light pattern scattered from the screen surface.

Based on the experimental results above, the structures of the device and heat sink were improved to attain the 100 W output power. The improvement was achieved by carrying out the following three steps.

As the first step, the structure of the heat sink was improved to increase the heat dissipation efficiency (Fig. 16) [21,22]. Furthermore, in order to reduce the heat generation, the device was driven by injecting a pulsed current with a duty ratio of 10:1. Since the pulse width was as large as 2 ms and the repetition frequency was as low as 50 Hz, this pulse current can be considered as a quasi-constant current.

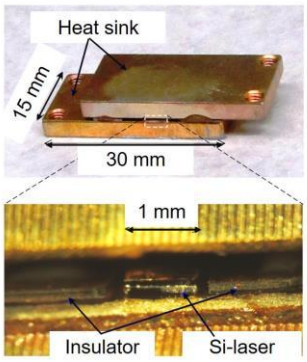

Fig. 16 Photograph of improved heat sink.

The relation between J and P_{out} is shown in Fig.17 and was consistent with the one estimated by the simulation (Fig. 12). This figure shows that the highest output power was 13 W (emitted from one end-facet). The value of J_{th} was maintained as low as 53 A/cm^2 (Fig.17). Figure 18 shows the light emission spectral profiles. The peak wavelength of the curve A is 1.34 μm. The FWHM of this curve is as wide as 455 nm, which indicates multi-mode operation because the mode was not controlled due to the large cavity size and to pulsed current injection.

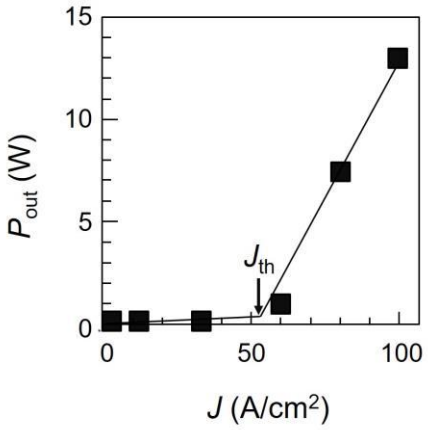

Fig. 17 Measured relation between J and P_{out} emitted from one end-facet of the Si crystal (the first step).

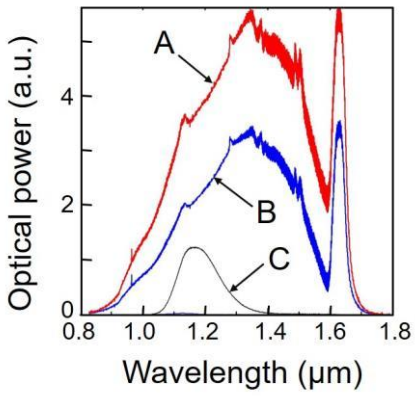

Fig. 18 Light emission spectral profiles (The first step).

Curve A, B, C are for injection current densities (duty ratio of 10:1, repetition frequency of 50 Hz) with pulse heights of 100 A/cm^2, 80 A/cm^2, and 60 A/cm^2, respectively. The origin of the sharp peak at 1.63 μm is not yet identified.

As the second step, the optical reflection-loss of the cavity was decreased by coating reflection films on the two end-facets of the cavity (the reflectivities were R_1=70 % and R_2=100 %) [23]. As a result, the value of J_{th} was decreased to 27 A/cm^2 (threshold current was 4 A), which was half of that in the first step. As shown in Fig. 19, the noise magnitude originated from the spontaneous emission below the threshold decreased to 1/10th to 1/100th that in the first step. Figure 20 shows the light emission spectral profiles, whose FWHMs were decreased to 150 nm. Furthermore, the inset of Fig. 20 shows that the lasing modes were resolved clearly due to the improved temporal coherence. The peak wavelength of these profiles was 1.18 μm, which was shorter than the peak wavelength (1.3 μm) of the light irradiated during the DP-assisted annealing. This was due to the wavelength dependence of the reflection films coated on the end-facets.

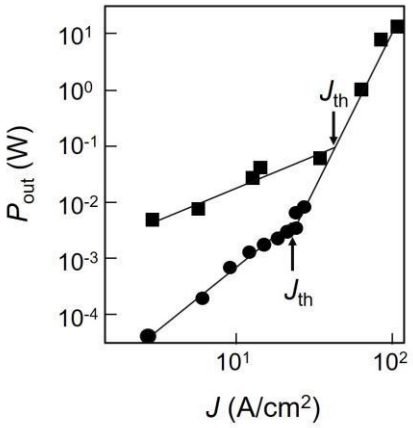

Fig. 19 Measured relation between J and P_{out}.

Closed circles are for the second step. Closed squares are identical to those in Fig. 17.

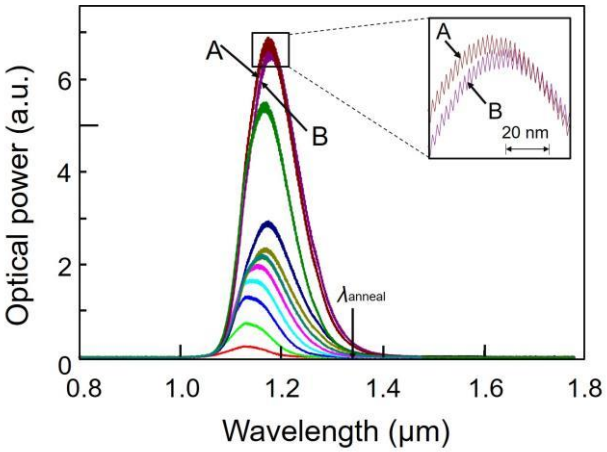

Fig. 20 Light emission spectral profiles (the second step).

Curves A and B are for injection currents with pulse heights of 4.2 A and 4.0 A, respectively.

As the last step, the implantation depth of the p-type dopant atoms was decreased from 2 μm to less than 1 μm so as to allow the device to be operated by a triangular-wave injection current (1 Hz repetition frequency). It should be pointed out that injection of such slow triangle-wave current is equivalent to constant current injection. The device length L was increased to 30 mm. Figure 21 shows the experimental results, demonstrating that the highest power achieved was 100 W. Through the comparison with the values represented by closed squares in this figure (the same as those in Fig. 17), it was confirmed that the value of J_{th} was maintained as low as the value realized in the first step.

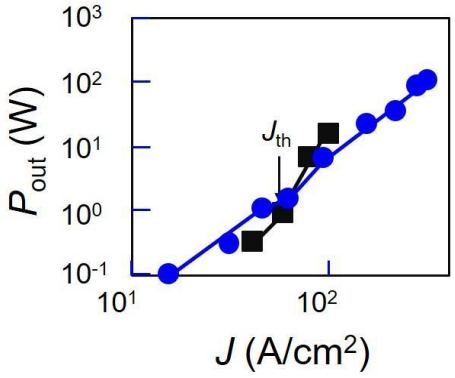

Fig. 21 Measured relation between J and P_{out} emitted from one end-facet of the Si crystal (the last step). Black squares are identical to those in Fig. 17.

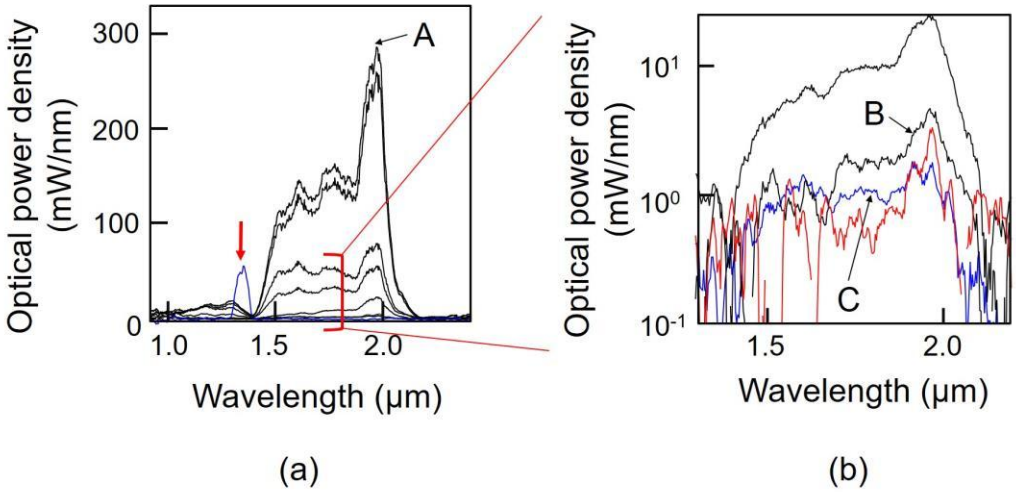

Fig. 22 Light emission spectral profiles (The last step).

The operating temperature was -20 °C. Curves A, B, and C are for triangular-wave injection currents (repetition frequency of 1 Hz) with peak current densities of 333 A/cm^2, 33 A/cm^2, and 17 A/cm^2, respectively. (a) The downward red arrow represents the wavelength of the light irradiated during the DP-annealing. (b) Magnified profiles of four curves in (a).

Figure 22 shows the light emission spectral profiles. The wavelength of the spectral peak is 1.95 μm, which is deviated from that (1.3 μm) of the light irradiated during the DP-annealing. The magnitude of this deviation is equal to $9E_{\text{phonon}}$, where E_{phonon} is the phonon energy. It means that nine phonons were involved for the momentum exchange with the electrons in the conduction band. It is expected that the peak wavelength can be tuned to 1.3 μm by modifying the wavelength-dependence of the reflectivity of the reflection films coated on the end-facets. An optical output power higher than 100 W and precise control of the lasing wavelength as well as lasing modes are expected by modifying the device structure

and the parameters for the DP-assisted annealing. Visible lasers are also expected to be fabricated by using crystalline SiC, also an indirect transition-type semiconductor that has been employed for fabricating visible LEDs [24].

4 Comparison with other type of lasers

The experimental results in Section 3 demonstrated that high P_{out} and low J_{th} were simultaneously realized as a result of the large optical gain and also the very low infrared absorption loss. Experimental progress made towards achieving this is summarized in Fig. 23.

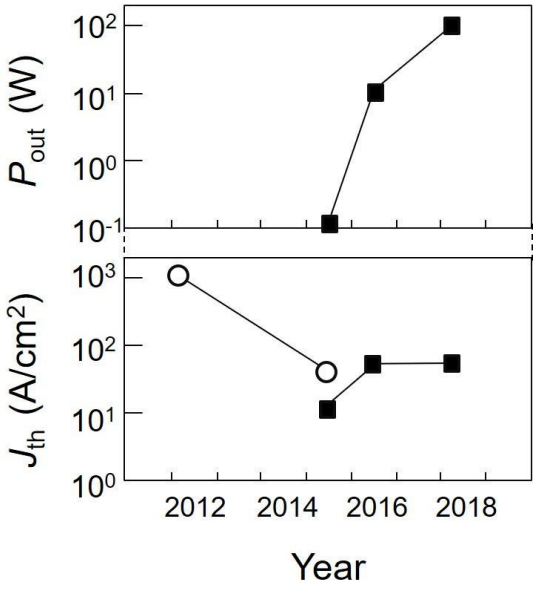

Fig. 23 Progress in increasing P_{out} and decreasing J_{th}, reviewed in this article.

Open circles and closed squares are for single-mode lasers (Section 2) and high-power lasers (Section 3), respectively.

Since a Si bulk crystal without a waveguide structure was used in Section 3, the structure of the present device is more similar to those of solid-state and gas lasers than those of conventional double heterojunction-structured semiconductor lasers [25,26]. Further similarities with solid-state and gas lasers can be found by referring to the magnitude of infrared absorption loss: In the case of solid-state and gas lasers, electronic transitions in the electronically isolated ions, atoms, and molecules are used for lasing. Therefore, even though direct electric current injection to these laser media is difficult, the absorption loss per unit volume is very low. Thus, a high optical output power can be obtained by increasing the size of the laser medium even though the photon density of the lasing light is low.

On the other hand, in the case of conventional semiconductor lasers, coupled electrons and holes in the conduction and valence bands, respectively, have been used for lasing. Therefore,

direct electric current injection to the laser medium is easy. An additional advantage is that the laser medium can be very small. However, the problem is that the absorption loss per unit volume is large, making it impossible to achieve high P_{out} and low J_{th} even though the photon density of the lasing light is high.

Considering the discussions above, the present Si laser is found to be similar to solid-state and gas lasers because an electronically isolated DP is used, which keeps the absorption loss per unit volume very low. Thus, the value of J_{th} can be decreased. Furthermore, the value of P_{out} can be greatly increased by increasing the size of the laser medium even though the photon density of the lasing light is low. An additional advantage is that electrons can be easily supplied by direct electric current injection, due to a low recombination loss in the Si crystal.

Finally, it should be pointed out that, early in the study of semiconductor lasers, it was found that the absorption loss in indirect transition-type semiconductors was low at low temperature, which was advantageous for inverting the electron population for lasing [27]. However, the disadvantage was that the magnitude of the population inversion was not sufficiently large for ensuring a large optical gain. Since this finding, it has been believed for a long time that indirect transition-type semiconductors were not appropriate for use as laser media. Instead, direct transition-type semiconductors have been predominantly used until now [28]. However, DP technology has realized the manifestation of large optical gain in indirect transition-type semiconductors, which is the secret to the dramatically high P_{out} and low J_{th} values realized by the present device made of Si crystal.

5 Summary

This article reviewed infrared Si lasers fabricated by DP-assisted annealing and capable of CW operation at room temperature. A basic device with a ridge waveguide operated in a single longitudinal-mode even though its cavity was as long as 500 μm. The lasing wavelength was 1.271 μm, which was evidence of the photon breeding phenomenon. The threshold current density J_{th} was 1.1 kA/cm^2. To decrease the value of J_{th}, a SOI substrate was used, and the waveguide structure was modified. As a result, J_{th} was decreased to 40 A/cm^2.

To realize a high-power Si laser device, a Si crystal with a large cross-section and a long length of 15 mm, and without a waveguide structure, was employed. The light emission spectral profile had phonon sidebands, which were evidence of photon breeding. The lasing wavelength, J_{th}, the external quantum efficiency, and the total optical output power were

1.37 μm, 12 A/cm^2, 9.0 %, and 220 mW, respectively. In order to realize an optical output power as high as 100 W, the device structure was improved by the following three steps. In the first step, the structure of the heat sink was improved, and the device was driven by injecting a quasi-constant current. As a result, the highest optical output power of 13 W was realized. The light emission spectral profile exhibited multi-mode operation with a peak wavelength of 1.34 μm. In the second step, high-reflection films were coated on both facets of the cavity. As a result, the noise magnitude below the threshold decreased to 1/10th to 1/100th.

As the last step, the cavity length was increased to 30 mm. By injecting a triangular-wave (1 Hz repetition frequency) current that was equivalent to injecting a constant current, an optical output power as high as 100 W was successfully obtained. The peak wavelength of the multi-mode lasing spectrum was 1.95 μm, which depended on the energies of nine phonons involved in the momentum exchange with electrons. It is expected that this wavelength can be tuned to 1.3 μm by controlling the wavelength dependence of the reflectivity of the high-reflection films coated on the end-facets.

The last part of this article compared the operating principle and performance of the present Si-lasers with those of conventional lasers.

References

[1] M. Ohtsu, *Silicon Light-Emitting Diodes and Lasers* (Springer, Heidelberg, 2016) pp.15-42.

[2] M. Ohtsu, *Dressed Photons* (Springer, Heidelberg, 2014) pp.1-88.

[3] M. Ohtsu, *Silicon Light-Emitting Diodes and Lasers* (Springer, Heidelberg, 2016) pp.65-82.

[4] D. Liang and J. E. Bowers, Nat. Photonics **4**, 511 (2010)

[5] H. Rong, R. Jones, A. Liu, O. Cohen, D. Hak, A. Fang, and M. Paniccia, Nature **433**, 725(2005)

[6] S. Saito, Y. Suwa, H. Arimoto, N. Sakuma, D. Hisamoto, H. Uchiyama, J. Yamamoto, T. Sakamizu, T. Mine, S. Kimura, T. Sugawara, and M. Aoki, Appl. Phys. Lett. **95**, 241101 (2009)

[7] M.G.A Bernard and G. Duraffourg, Phys. Status Solidi, **1**, 699 (1961).

[8] T. Kawazoe, M. Ohtsu, K. Akahane, and N. Yamamoto, Appl. Phys. **B 107**, 659 (2012)

[9] H.Tanaka, T. Kawazoe, M. Ohtsu, and K. Akahane, Fluoresc. Mater. **1**, 1 (2015)

[10] M. Ohtsu, *Silicon Light-Emitting Diodes and Lasers* (Springer, Heidelberg, 2016) pp.16-19.

[11] W. J. Choi, P. D. Dapkus, and J. J. Jewell, IEEE Photon. Tech. Lett., **11**, 1572 (1999)

[12] T. Tanbun-Ek, N. A. Olsson, R. A. Logan, K. W. Wecht, and A. M. Sergent, IEEE Photon. Tech. Lett., **3**, 103 (1991)

[13] M. Ohtsu, Y. Teramachi, and T. Miyazaki, IEEE J. Quantum Electron., **24**, 716 (1988)

[14] M. Ohtsu and Y. Teramachi, IEEE J. Quantum Electron., **25**, 31 (1988)

[15] H. Tanaka, T. Kawaze, and M. Ohtsu, Appl. Phys. B, **108**, 51 (2012).

[16] H. Tanaka, T. Kawazoe, M. Ohtsu, K. Akahane, and N. Yamamoto, Appl. Phys.A **121**, 1377 (2015).

[17] Z. I. Kazi., T.Egawa, T. Jimbo, and M. Umeno, IEEE Photonics Technol. Lett. **11**, 1563 (1999)

[18] G.P. Agrawal and N.K. Dutta, *Semiconductor Lasers*, 2nd ed. (Van Nostrand Reinhold, New York, 1993).

[19] H. Tanaka, T. Kawazoe, and M. Ohtsu, Abstract of the 63st JSAP Spring Meeting, March 2016, Tokyo, Japan, paper number 19a-S622-8.

[20] H. Tanaka, T. Kawazoe, M. Ohtsu, K. Akahane, and N. Yamamoto, Abstract of the 76th JSAP Autumn Meeting, September 2015, Nagoya, Japan, paper number 16p-2G-8.

[21] T. Kawazoe, K. Hashimoto, and S. Sugiura, "High-power current-injection type Silicon laser using nanophotonics," Abstract of the EMN Nanocrystals Meeting, October 17-21, 2016, Xi'an, China, pp.9-11 (paper number 03).

[22] T. Kawazoe, S. Sugiura, and M. Ohtsu, Abstract of the 64th JSAP Spring Meeting, March 2017, Yokoyama, Japan, paper number 15a-F202-9.

[23] T. Kawazoe, K. Hashimoto, and S. Sugiura, Abstract of the 65th JSAP Spring Meeting, March 2018, Tokyo, Japan, paper number 19p-F310-14.

[24] M. Ohtsu, *Silicon Light-Emitting Diodes and Lasers* (Springer, Heidelberg, 2016) pp.83-101.

[25] M. Ohtsu, *Coherent Quanatum Optics and Technology* (KTK Scientific and Kluwer Academic, Tokyo, Dordrecht, Boston, London, 1992) pp.49-81.

[26] M. Ohtsu, *Highly Coherent Semiconductor Lasers* (Artech House, Boston, 1992) pp.7-60.

[27] J.R. Singer (ed.), *Advances in Quantum Electronic*s, (Columbia University Press, New York, 1961) pp.456-506.

[28] W.P. Dumke, Phys. Rev. **177**, 1559 (1962).